infrastructures

Article

On the Effectiveness of Vibration-Based Monitoring for Integrity Management of Prestressed Structures

Marco Andrea Pisani, Maria Pina Limongelli, Pier Francesco Giordano * and Mattia Palermo

Department of Architecture, Built Environment and Construction Engineering, Politecnico di Milano, Piazza Leonardo da Vinci 32, 20133 Milan, Italy; marcoandrea.pisani@polimi.it (M.A.P.); mariagiuseppina.limongelli@polimi.it (M.P.L.); mattia.palermo@mail.polimi.it (M.P.)
* Correspondence: pierfrancesco.giordano@polimi.it

Abstract: In this paper, the effectiveness of vibration-based tests for the detection of damages for prestressed concrete beams is investigated. Despite large research efforts, discrepant and sometimes contradicting conclusions have been drawn regarding the efficacy and reliability of vibration-based monitoring for prestressed structures. Herein, a contribution to this discussion is provided by tackling the problem from a different perspective. Specifically, the question that this paper intends to answer is: "Do vibration-based tests support decision-makers in integrity management operations for prestressed elements?" The discussion is carried out by comparing the performance of prestressed and ordinary reinforced concrete beams with similar capacities. Both analytical and numerical case studies are considered. Results show that, for prestressed beams, in contrast to reinforced concrete beams, modal parameters can provide information regarding damage only when the structure is close to its ultimate conditions. This makes this information hardly useful for integrity management purposes and the effectiveness of vibration-based tests questionable for this type of structural element.

Keywords: vibration-based monitoring; structural health monitoring; damage detection; prestressed beams; bridge management

check for updates

Citation: Pisani, M.A.; Limongelli, M.P.; Giordano, P.F.; Palermo, M. On the Effectiveness of Vibration-Based Monitoring for Integrity Management of Prestressed Structures. *Infrastructures* **2021**, *6*, 171. https://doi.org/10.3390/infrastructures6120171

Academic Editor: Joan Ramon Casas Rius

Received: 8 November 2021
Accepted: 29 November 2021
Published: 3 December 2021

1. Introduction

Vibration-based methods for structural health monitoring are used to verify structural integrity using the response to vibrations [1,2]. This enables identification and implementation, in a timely fashion, decisions regarding remedial actions to counter deterioration, damage, and extreme loads before they pose a threat to the structural integrity or reduce the functionality of the asset. The dynamic behavior of structures is stiffness dependent, thereby vibration-based methods can detect damages induced by stiffness losses. One of the major advantages of these methods is the possibility to detect damage at a global level, using sensors not necessarily deployed close to the location of damage, the position of which may be unknown [3–5]. The behavior of prestressed beams has been the object of several studies aimed at investigating the possibility of detecting losses of prestress, corrosion, and localized impacts through the analyses of their dynamic behavior. Losses of prestress generally do not produce a reduction of the section strength. Instead, corrosion and localized impacts produce a reduction of the steel and/or concrete area. In principle, the employment of vibration-based methods should be feasible to identify the corresponding stiffness losses. However, this is not always the case, as shown by several experimental investigations focused on the assessment of the sensitivity to damage of features extracted from the response to vibration. Several authors have repeatedly reported the difficulty in using modal frequencies to identify de-tensioning of the prestressing cables. Kato and Shimada [6] published the results obtained by measuring ambient vibrations on a prestressed concrete bridge during a static failure test. The evolution of the frequency of the first vertical mode at the increase of the load applied at midspan pointed out a negligible variation, which the authors attributed to cracking of the concrete, up to the yielding of the steel wires. Beyond this limit, a sudden decrement of the natural frequency was observed. Hop [7] tested 18 prestressed beams to determine the effect of the degree of prestressing on frequency and damping. The author points out that a reduction in vibration frequency is observed when consecutive cracks appear in the beams. Some years later, Saiidi et al. [8] performed impact and ambient vibration tests on a post-tensioned concrete bridge for which they compared the prestress losses measured directly on the cables with the variations of the modal frequency. Results show variations of the modal frequency lower than 1% for a loss of tension around 8%, which the author attributed to the opening of microcracks. This is also confirmed by the experimental results obtained more recently by other researchers. For example, Unger et al. [9] report the results of impact tests performed on a post-tensioned concrete beam gradually damaged by increased static loading applied at midspan. Due to the closing of the cracks caused by the prestressing, only slight changes of the modal frequencies were detected before the yielding of reinforcement. Similar conclusions are reported in the works by Capozucca [10] and Di Evangelista et al. [11]. Negligible variations of modal frequencies are also reported in [12] for beams prestressed by external tendons and tested with impact hammer tests. Similarly, in [13], based on the results of experimental modal analyses performed on a laboratory beam with decreasing values of post-tensioning force, the authors conclude that there is no indication of any relationship between post-tensioning load magnitude and fundamental bending frequency. Wang et al. [14] reported the results of impact tests carried out on five prestressed concrete beams with parabolic or straight cables in different conditions—before prestressing, prestressed before grouting, and prestressed after grouting. These conditions were meant to simulate the behavior of different types of beams—simply reinforced, unbonded prestressed, and bonded prestressed. Results showed that the first modal frequency of beams with straight tendons did not exhibit any variation with the increase of prestressing force. The authors, who describe a variation of modal frequencies with prestress force in a prestressed beam tested in the laboratory, emphasize that it is accompanied by the cracking of concrete. These results were confirmed by an experimental campaign carried out on a post-tensioned concrete beam [15]. Results showed that variations of the first and second modal frequencies with the tension in the prestressing cables were hardly detectable until the formation of cracks in the beam. The scarce sensibility of traditional modal parameters (e.g., modal frequencies) to damage in prestressed beams is also discussed in more recent publications [16,17].

All the previous investigations were carried out on single prestressed beams tested in a laboratory. In the literature, similar results are reported for vibration tests performed on-site on bridges with controlled losses of tension in prestressed beams. In the realm of the SIMCES project, De Roeck performed full-scale tests on the Swiss Z24 bridge [18] with two post-tensioned girders for which a loss of tension was simulated through the cutting of six post-tensioning tendons. Based on the analyses of the dynamic response recorded during ambient vibrations, the authors remarked that a loss of prestress results in a measurable change in eigenfrequencies only if it is accompanied by originating cracks. The same result was obtained through the analyses of responses recorded on the S101 bridge [19,20], a post-tensioned flyover of three spans near Vienna. Before demolition, an experimental campaign of ambient vibration tests was executed, artificially simulating the loss of tension in the cables through the progressive cut of several tendons and recording the response to vibrations. Once again, the analyses of the response to vibrations were unable to identify this type of damage due to the negligible variation of the damage indicators extracted from these data. Recently, Abdel-Jabel and Glisic [21] published a detailed overview of available methods for monitoring prestressed forces. Based on the outcome of several studies, they analyzed the application of vibration-based methods for the detection of prestress losses, concluding that, in the case of uncracked beams, changes in prestress forces do not affect natural frequencies. Nowadays, research on dynamic monitoring of prestressed concrete structures remains active [22–25]. The goal of these projects is usually to verify and validate the effectiveness of vibration-based methods for damage detection.

In this paper, we consider the problem from a different perspective that is not limited to the investigation of the sensitivity of vibration-based damage features to detect damage, but extends the discussion to the practical use of the information extracted from this type of test. The information from inspections, tests, or monitoring carried out on any structure is meant to support decisions relevant to its integrity management. To this aim, precise and accurate, i.e., correct, information is needed. However, correctness is not enough to state that the information can effectively support integrity management. The main question we aim to answer in this paper is if the information acquired using vibration-based monitoring for prestressed components is effective in supporting integrity management. The discussion is carried out through the comparison of the performance of reinforced concrete and prestressed beams at the onset and the development of a deterioration that causes a loss of concrete area and thereby variations of the beam stiffness. The structure of the paper follows.

In Section 2, the impact of uncertainties on the information provided by vibration-based tests, specifically modal frequencies, is briefly discussed to describe the sources that can reduce their effectiveness as damage features. Using a very simple analytical model in Section 3, the effect of damage on several characteristic parameters of the cross-section of an ordinary and a prestressed concrete section is investigated to describe their differing sensitivity to losses of steel area. A more refined numerical model is used in Section 4 to compare the performance of the two types of sections, damaged by corrosion, in terms of modal frequencies and probability of failure. Based on the results of this investigation, a discussion regarding the role and benefits of the information provided by vibration-based tests for reinforced and prestressed sections is reported in Section 5. The conclusions end the paper.

2. Effect of Uncertainties on Modal Parameters

In civil engineering contexts, the identification of modal frequencies from vibration-based tests is commonly carried out through Operational Modal Analysis (OMA) techniques, which allow estimating the modal parameters of a structure by measuring solely the vibrational response [26]. Several OMA techniques exist, which generally are classified into time domain and frequency domain methods. Time-domain methods rely on the analysis of the response time histories, such as Stochastic Subspace Identifications (SSI) methods [27] or the Hilbert–Huang Transform [28]. Frequency domain methods are based on the Fourier transform of the response, such as the Enhanced Frequency Domain Decomposition (EFDD) method [29]. Additionally, mixed time–frequency methods exist, such as the recently proposed Clustered Filter Bank method [30].

The vibration-based identification process, from response measurement to modal frequencies estimation, is an experimental process subjected to several uncertainties introduced by several sources, not the least environmental conditions, such as temperature and humidity (moisture content), which can induce daily or seasonal variations of the modal frequencies that easily exceed 5–10% [26–30]. Therefore, changes of the indicators due to temperature can mask or mistakenly denounce damage that induces variations of modal frequencies within this range. Several methods based on regression models, pattern recognition, or machine learning techniques have been proposed to account for or remove these effects [31–33]. Similarly, operational variability due to traffic (mass and velocity of vehicles) may also induce variations of the modal parameters to higher than 5% [34,35] particularly for bridges with a small mass ratio between the structure and the vehicles. Due to the relevant variation of the mass, modal parameters can change, leading to incorrect identification of damage in a healthy structure. Other sources of uncertainty in measured data are relate to: Instrumental systematic or random errors related to the characteristics and implementation of the acquisition and transmission hardware (e.g., sensors, acquisition system, transmission cables); the mathematical models used to extract modal frequencies from the structural response (for example, that the excitation is a broadband stochastic process—e.g., a white noise—not strictly and always verified in case of ambient vibrations); approximations related to signal processing (for example, signal truncation when working with assumed infinite length of the recorded signals); and errors connected with the nonlinear structural behavior whenever this is not accounted for in the interpretative models considered. The effect of these uncertainties is to induce a variability, which can reach values higher than 5% of the estimated modal frequency that is much higher, as will be shown in Sections 3 and 4, with respect to the variation of frequency produced by corrosion in a prestressed beam.

3. Effect of Damage in Ordinary and Prestressed Concrete Sections

In this paper, damage is intended as the reduction of steel or concrete area. This type of damage, due, for example, to corrosion or by an impact, causes reduction of stiffness that in principle could be detected using vibration-based methods of damage identification and, specifically, investigating the variation of the modal frequencies with damage.

Prestressing is a self-induced, self-equilibrated stress distribution resulting from controlled noncompatible strains between the steel cables and the surrounding concrete. In bonded prestressing, this concept applies at every cross-section of the beam [36]. This stress distribution is conceptually similar to the initial residual stress in hot rolled steel wide-flange shapes that is developed by the manufacturing processes of hot rolling and subsequent cooling [37]. Because of this, the n-th natural frequency, ω_n, of a simply supported beam prestressed with bonded tendons is determined through the following equation [38]:

$$\omega_n = n^2 \pi^2 \sqrt{\frac{E_c J_i}{m L^4}} \tag{1}$$

where E_c is the elastic modulus of the concrete, $E_c J_i$ is the equivalent flexural rigidity of the composite section (concrete and tendons), L is the span of the beam, and m is the mass for unit length.

3.1. Variation with Damage of the Flexural Rigidity in Ordinary and in Prestressed Sections

To discuss the different impacts of damage on reinforced and prestressed concrete sections, the variation of the flexural rigidity is herein briefly discussed. The section inertia moment J_i reads:

$$J_i = J_c^* + m \cdot \sum_i {y_{si}}^2 \cdot A_{si} \tag{2}$$

where J_c^* is the moment of inertia of the compressed concrete computed with respect to the principal axis x of the composite cross-section that lies on its neutral axis only for reinforced concrete sections, A_{si} is the area of the steel bar at a distance y_{si} from the x-axis, and m is the modulus of elasticity transformation coefficient for steel to concrete.

In a reinforced concrete section, the concrete compressed area depends on the neutral axis position. A reduction of the steel area causes a change of the neutral axis position and thereby a reduction of the term J_c^* in Equation (2). In a fully prestressed section, the entire cross-section is compressed; thus, the term J_c^* in Equation (2) depends on the steel area. This results in a very small variation of the flexural stiffness due to the variation of the second term in Equation (2) and constitutes a crucial difference between reinforced concrete and prestressed concrete regarding the possibility to use vibration-based monitoring to detect this type of damage. When increasing the tension steel area, the difference in the performance of the two types of sections becomes even higher due to the differing dependence of the section inertia moment J_i on the tension steel area. The percentual reduction $p(\gamma)$ of the flexural stiffness with damage (loss of the tension steel area) reads:

$$p(\gamma) = \frac{J_i - J_{i,\gamma}}{J_i} \tag{3}$$

where the reduced tension steel area is modeled as γA_s, with $(0 \le \gamma \le 1)$.

For a given value of γ, the last term on the right side of Equation (2) decreases proportionally to A_s. This occurs both for reinforced concrete and for prestressed sections. For a fully prestressed section, where the entire concrete section is compressed, J_c^* $J_{c,\gamma}^*$ (the difference is due to a slight shift of the x-axis), whereas for a reinforced concrete section the term $J_{i,\gamma}$ decreases with γ; thus, the variation of the difference $J_c^* - J_{c,\gamma}^*$ is not negligible. For the sake of simplicity, and without any loss of generality, this variation is illustrated in the following with reference to a rectangular section. In Figure 1A, the variation of the compressed concrete area (in red) and of the section inertia moment (in blue) with the steel geometric ratio A_s/bh are reported. The area and the inertia moment of the compressed concrete are normalized to the area and the inertia moment of the gross concrete section, respectively. In the figures, the following notations are used: b and h are the width and the height of the concrete section, respectively, A_c^* is the compressed concrete area, δ is the nondimensional concrete cover, and σ_c and σ_s are normal stress in concrete and steel bars, respectively.

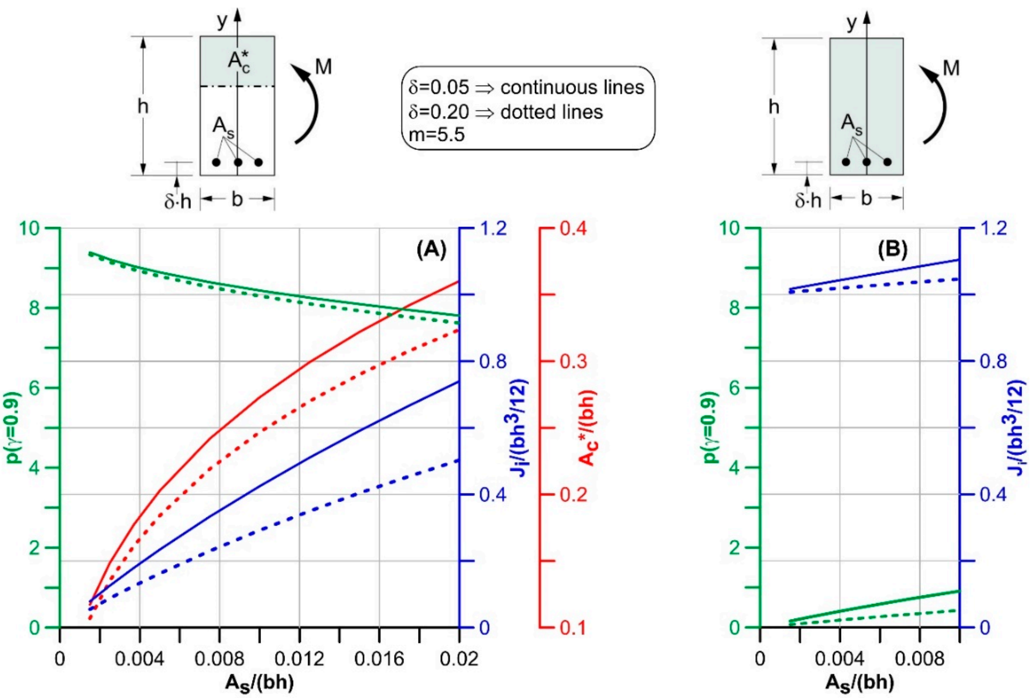

Figure 1. Rectangular cross-section: (**A**) reinforced concrete and (**B**) prestressed concrete.

To consider a wide range of geometric dimensions of the section, two values (δ equal to 5% and 20%) are considered for the ratio between the concrete cover and the gross section height. Considering a value of the concrete cover of 5 cm, these two values cover a range of section height between 25 cm and 100 cm. The geometric steel ratio A_s/bh between the steel area and the gross concrete section is considered in the range 0.1% and 2% for a reinforced concrete section and in the range 0.1% and 1% for a prestressed section. These values cover the entire spectrum of steel and tendons areas used in common practice. For prestressed concrete, the maximum geometric steel ratio of the tendons considered is half the value considered for the reinforced concrete section. This choice comes from the observation that the strength of the prestressing tendons is at least double (e.g., for Dywidag bars) with respect to that of a rebar and that a correct design requires the yielding of the tension reinforcement (ordinary or prestressed) before the ultimate load is reached. The continuous and dotted lines are relevant to the two different assumptions regarding the concrete cover-to-section height ratios. As expected, both the compressed concrete area (in red) and the section inertia moment (in blue) increase with the steel area. It is noted that the increase of the compressed area A_c^* is faster (the curve is steeper) for lower values of the steel area. The figure also reports (shown in green) the percentual variation p due to a loss of 10% of steel area ($\gamma = 0.9$).

In Figure 1B, the normalized compressed concrete inertia moment (in blue) and the percentual reduction of the inertia moment are reported for a prestressed section. The normalized compressed concrete area in this case has a constant unit value. The comparison of the two figures shows two main differences. The first is that similar values of the steel area correspond to values of the section inertia moment of the prestressed section of about three times that of the reinforced concrete section. This represents a peculiarity of prestressed beams, where values of the geometric steel ratio are in the common range 0.15–1%, and the area of concrete amounts to values between 95.2% and 99.2% of the effective area of the section $A_i = A_c + m \cdot \sum_i A_{si}$ (assuming $m = E_s/E_c \simeq 5.5$). The second difference is the trend of the percentual variation p that decreases for the reinforced concrete section and increases for the prestressed sections. This parameter quantifies the impact of damage on the inertia moment of the section thereby the two trends indicate that for a reinforced concrete section the increase of steel area decreases the impact of damage; for a prestressed section, the opposite occurs. Furthermore, the variation is negligible—lower than 0.5%—for a prestressed section and of 4–5% for a reinforced concrete section.

3.2. *Variation with Damage of the Modal Frequencies of an Ordinary and a Prestressed Beam*

The comparison of the reinforced and prestressed sections reported in the previous section shows that damage with the same severity, loss of 10% of steel area in the example considered, produces very different variations of the section inertia moment, close to 8–10% for a reinforced concrete section and around 0.1–1.5% for a prestressed section.

These variations induce changes in the beam modal frequencies which, in the case of a beam with a constant transversal section, can be estimated using Equation (1). This equation provides a good estimate of the modal frequency of a prestressed beam when the area of the tension reinforcement is constant along its length. It also provides a very good approximation when the area of the tension reinforcement is not constant, as shown by Figure 1B, where a 10% reduction of the tension reinforcement implies a reduction lower than 1% of the local inertia moment of the beam. Moreover, Equation (1) also provides a good estimate of the modal frequency for a reinforced concrete beam, since in any cross-section the depth of the neutral axis, and thereby the resisting concrete section, does not change with the bending moment.

According to Equation (1), modal frequencies are proportional to the square root of the inertia moment; thus, the variation of the modal frequencies for the rectangular section considered in Section 3 are close to 4–5% and 0.07–1.5% for a reinforced and a prestressed beam, respectively (see Figure 2).

As mentioned in Section 2, the process to extract modal frequencies using experimental or operational modal analyses is affected by several uncertainties that can hamper a reliable detection of damage caused by a reduction of the steel area—induced, for example, by corrosion based on the values of the modal frequencies.

If corrosion does not affect uniformly the beam along its length, the frequency variation is even lower since the variation of the inertia moment occurs only in the sections affected by corrosion. It can be concluded that the use of modal frequencies as damage features to detect steel losses due to corrosion cannot be effective because the associated stiffness changes are not large enough to be detected under real-world conditions. These results confirm and provide a quantitative and formal justification to the outcomes of the several experimental campaigns referenced in Section 1, which pointed out the scarce efficiency of vibration-based damage detection for prestressed beams.

In the next section, this result will be confirmed through more refined numerical analyses on prestressed and reinforced concrete beams subjected to corrosion.

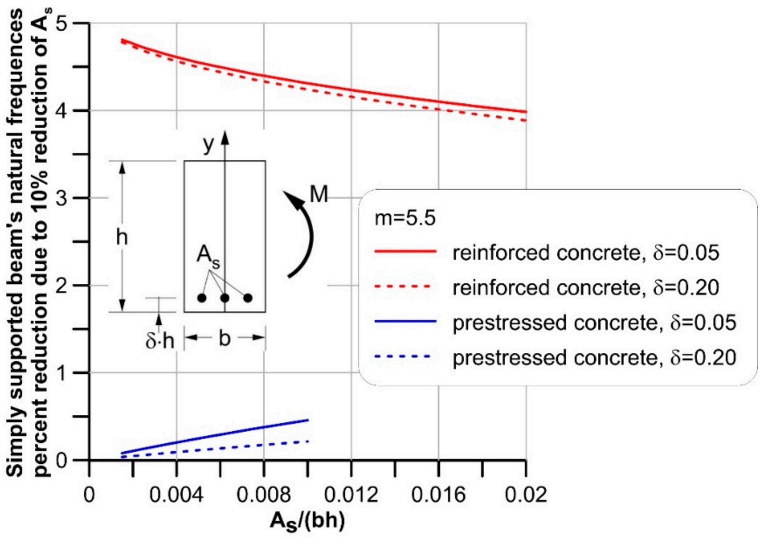

Figure 2. Modal frequencies versus the area of the tension reinforcement.

4. Numerical Analyses of Ordinary and Prestressed Concrete Sections Exposed to Corrosion

4.1. Numerical Model of the Sections Damaged by Corrosion

In this section, the performance of a prestressed and of a reinforced concrete beam exposed to corrosion that leads to loss of steel area and concrete spalling is compared. A bridge deck supported by seven prestressed AASHTO/PCI I-beams type III 20 m long and placed 1.7 m from one another is considered (Figure 3A). The deck was designed for a previous study [39] to bear the design loads provided by the Eurocodes [40]. The performance of these prestressed beams is compared with that of reinforced concrete beams described in Figure 3B and designed with the same ultimate moment resistance. Despite their higher flexibility, the reinforced concrete beams satisfy the deformation requirements (i.e., deck deformation limit) of the AASHTO standards [41].

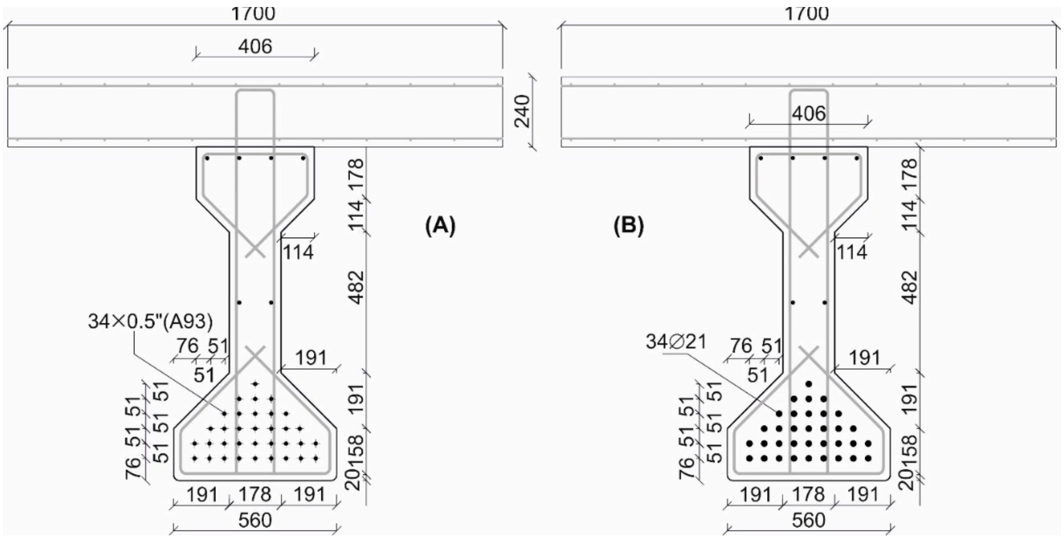

Figure 3. (**A**) AASHTO/PCI I-beams type III and (**B**) the reinforced concrete homologous beam (dimensions are in mm).

The strength class of the concrete of the precast prestressed beam is C50/60 with characteristic compressive strength of 50 MPa and Young's modulus of 37 GPa. The slab is cast in place with concrete of strength class C35/40 and elastic modulus of 34 GPa. Tendons are seven wires 0.5″ strands (area = 93 mm^2). Their characteristic yielding stress is $f_{p0.1k}$ = 1670 MPa, the strength is f_{pk} = 1860 MPa, the strain at ultimate is 3.5%, and Young's modulus is 195 GPa. The rebars of the reinforced concrete beam have characteristic yielding stress of f_{yk} = 450 Mpa and an elastic modulus equal to 200 GPa. The beams are designed according to Eurocode 2 [42].

The design of the cross-section of the beams takes into account the construction in stages [43]. In the first phase, the beam alone carries its self-weight, the self-weight of the slab (cast in situ), and of a midspan crossbeam. The distributed load is equal to 19.20 kN/m and the concentrated midspan load is 12.30 kN. In the second phase, after concrete curing, the slab participates in all the load increases.

Variable loads and the relevant masses have been neglected in the evaluation of the modal frequencies due to their negligible values with respect to the permanent and quasi-permanent loads due to asphalt concrete and finishes that apply a uniform load of 5.10 kN/m.

Two different exposure conditions were considered to cover a wide range of real-world cases, namely: (1) a very aggressive environment leading to concrete heavily contaminated by chloride and 95–98% Relative Humidity (RH) and (2) a moderately aggressive environment with concrete contaminated by chloride and RH lower than 90%. It is highlighted that chlorides are not the only cause of corrosion. For instance, sulfate attacks [44,45] greatly affect concrete elements and can reduce their elastic modulus [46]. The time of initiation of corrosion T_i was computed according to the following equation [47]:

$$T_i = \frac{C_p^2}{4D}\left[erf^{-1}\left(\frac{C_{cr}-C_s}{C_0-C_s}\right)\right]^2 \tag{4}$$

where C_p is the thickness of the concrete cover. The definition and values of the parameters in Equation (4) are listed in Table 1. Their discussion is outside the scope of this publication, but the interested reader can refer to papers [47–49] for more details. The corrosion rate, needed to estimate the reduction of the steel area at the progression of corrosion in time, was set to 0.7 mm/year for the very aggressive environment and 0.087 mm/year for the moderately aggressive one [50].

Table 1. Definition and values of the parameters in Equation (4).

Parameter		Very Aggressive Environment	Moderately Aggressive Environment
C_s = Chloride surface content		2.8	1.37
C_0 = Chloride surface content		0	0
C_{cr} = Chloride surface content	RC beam	0.6	0.6
	PC beam	0.2	0.2
D = Chloride surface content		$5'10^{-12}$	$5'10^{-12}$

The age of the beam at spalling was determined following the Liu and Weyers approach [51]. Spalling is assumed to occur when the thickness of the corrosion products leads to the limit value of the pressure at the concrete/rust products interface. The value of the limit pressure depends on the diameter of the tension reinforcement and the tensile strength of the concrete. Values of 13.03 and 21.55 MPa were assumed herein for the reinforced concrete and the prestressed beams, respectively [48]. The RC slab is reinforced with glass fiber reinforced polymer rebars; thus, it was considered not exposed to corrosion.

The evolution of damage is described in Figure 4. Corrosion starts from the bottom, leftmost, and rightmost tension reinforcement (1st damage phase); later it reaches the remaining peripherals tension rebars (2nd damage phase) until spalling of the bottom concrete cover occurs (3rd damage phase), followed by spalling of the side concrete cover of the bottom flange (4th damage phase). The last stage corresponds to the halving of the reinforcement area, thereby to a value of the resisting bending moment lower than the maximum service moment at midspan.

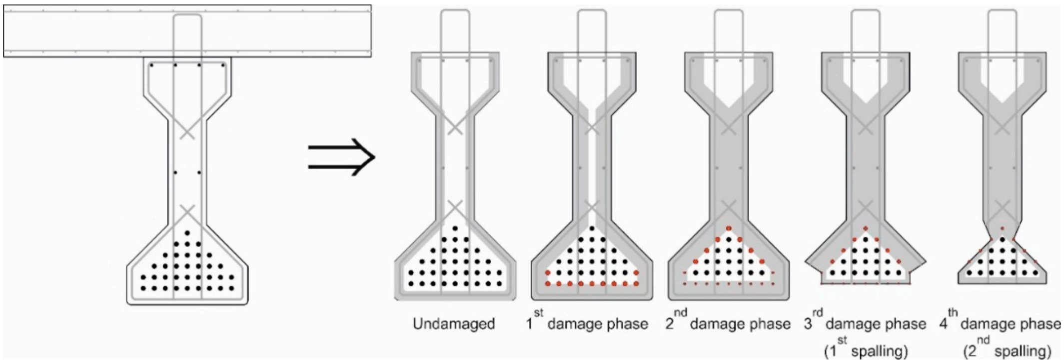

Figure 4. Evolution of damage (the grey shading indicates the carbonated concrete).

4.2. Numerical Model of the Sections Damaged by Corrosion

Figure 5A describes the evolution through time of the geometric and mechanical characteristics of the reinforced concrete beam as a function of the tension reinforcement area decrease due to corrosion. The graph must be read through the colors: each curve refers to an axis of the same color. The results shown in the figure agree with what was expected: the second moment of area, and therefore also the first natural frequency of the beam, gradually decreases as the area of the tension reinforcement decreases (as a result of corrosion). The ultimate resistant moment also decreases. In particular, at the first spalling the ultimate resisting moment is only slightly higher than the maximum service bending moment. The variation of the section inertia moment J_i is significant and progressive.

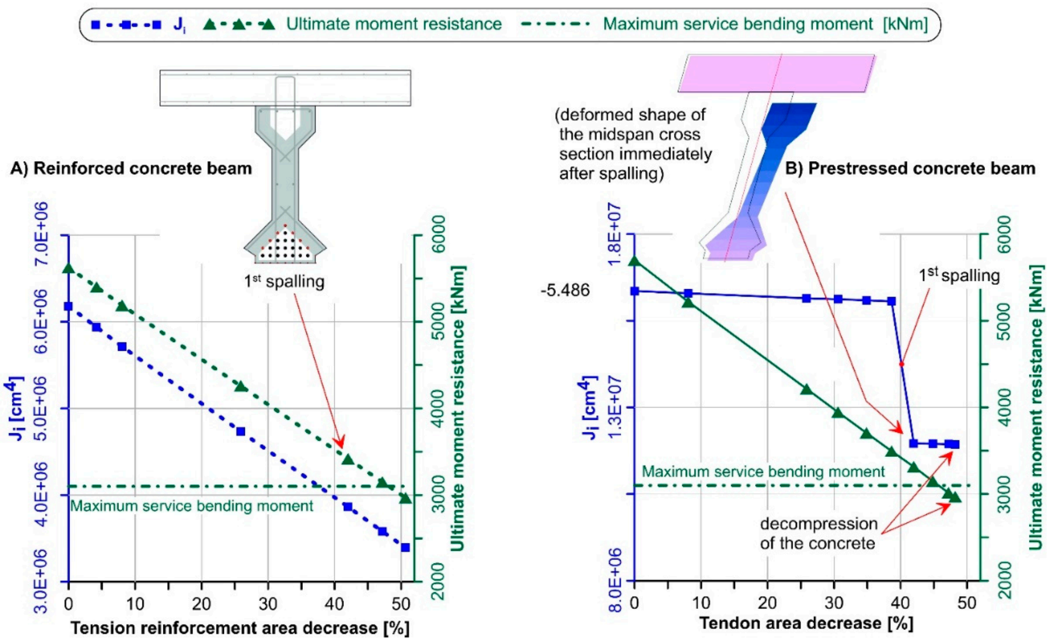

Figure 5. Evolution through time of the geometric and mechanical characteristics of the beams.

Figure 5B shows the radically different behavior of the prestressed beam. The ultimate moment resistance decreases progressively with the reduction of the area of the tendons due to corrosion. The section inertia moment, and thereby the frequency, do not change significantly until the first spalling of the bottom concrete cover occurs, inducing a sudden change in these parameters. The further evolution of corrosion leads to the decompression of the section, and from this point on, a progressive, quite fast, variation of the frequency also occurs. It is noted that the first spalling leads to a value of the ultimate moment resistance which is only 7% higher than the maximum service bending moment (initially, i.e., before damage, it was 84% higher). In this condition, the reliability of the beam is close to zero. Looking at the deformed shape of the midspan cross-section of the beam immediately after the first spalling (depicted in Figure 5B), note that the section is entirely compressed even after spalling has occurred and that the strain inside the reinforced concrete slab is much lower than the one that is present at the top of the I beam, where a self-equilibrated stress distribution due to prestressing is acting.

Figures 6 and 7 are intended to compare the behavior of the reinforced and prestressed beams while corrosion, represented by the beam age reported on the x-axis, advances. The continuous curves refer to the prestressed concrete beam and the dotted curves to the reinforced concrete beam. The red curves report the percent decrease of the tension reinforcement area, the green curves report the values of the residual ultimate moment and finally, the magenta curves report the frequency variation. Each of these curves refers to the ordinate axis of the same color.

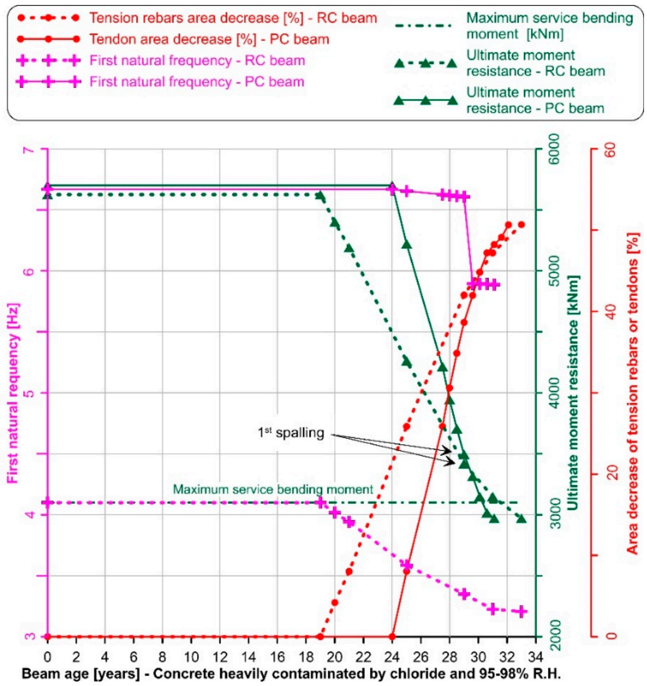

Figure 6. Very aggressive environment. The behavior of the beams at the progress of corrosion.

The comparison of the two figures shows that in reinforced concrete corrosion starts earlier, but degradation progresses more slowly than in the prestressed beam. The earlier start of corrosion depends on the presence of cracking in reinforced concrete, whereas the reduction of the mechanical performance of the tendons is much faster (almost double) than that of the rebars due to the lower steel area of the tendons with respect to the rebars.

Figure 6 shows that in the case of a highly aggressive environment contaminated by chlorides with an RH between 95 and 98% ($v = 0.701$ mm/year), the first spalling is reached in 29 years, both for reinforced concrete and prestressed concrete. This time is certainly far less than the 100 years of intended life prescribed by the standards. In the case of a moderately aggressive environment, the first spalling occurs after 80 and 45 years from the start of corrosion for reinforced concrete and prestressed concrete, respectively. Assuming that the performance of the beam is not acceptable after the first spalling occurs and considering the different ages of the two beams at corrosion start, the length of the service life is $t = 102$ years and $t = 85$ years for reinforced and prestressed concrete, respectively. While for the reinforced concrete bridge this value is equal to the one required by the standards, for the equivalent prestressed bridge the value is lower than the limit prescribed by the Eurocodes.

In the introduction of this paper, the scarce efficacy of vibration-based tests for damage detection in prestressed elements was noted with reference to the outcomes of several experimental campaigns. The main issue stems from the difficulty of measuring significant frequency variations for reductions—even significant—of the element load-carrying capacity. The previous numerical example shows that the main reason for the scarce sensitivity of modal frequencies to corrosion dwells in the negligible influence of this type of damage on the geometrical characteristics of the prestressed concrete section. This result is general and independent of the beam geometry. In Figure 8, the variation of the ultimate moment with the decrease of the tendon area obtained for the prestressed beam in the previous numerical example is compared with the experimental values obtained in [52] for a fully prestressed specimen. Despite the radical difference in geometry of the section and the fact that the AASHTO beam is connected to a reinforced concrete slab, the behavior is almost identical.

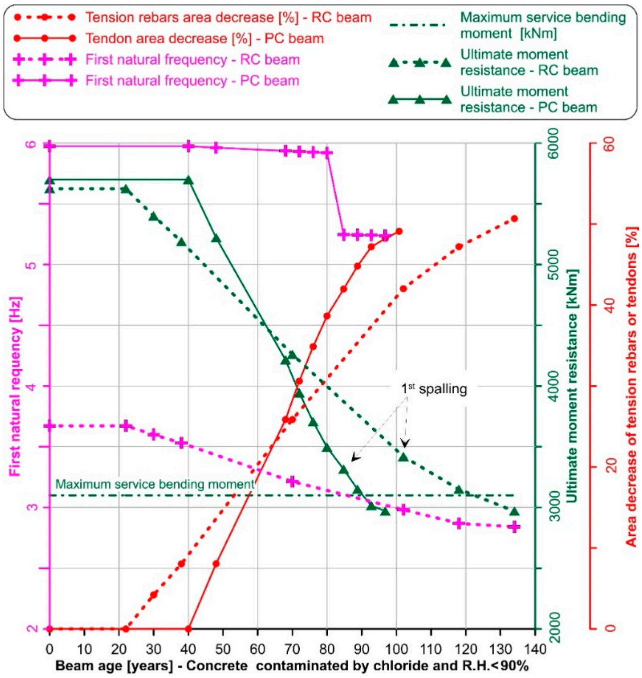

Figure 7. Moderately aggressive environment. The behavior of the beams at the progress of corrosion.

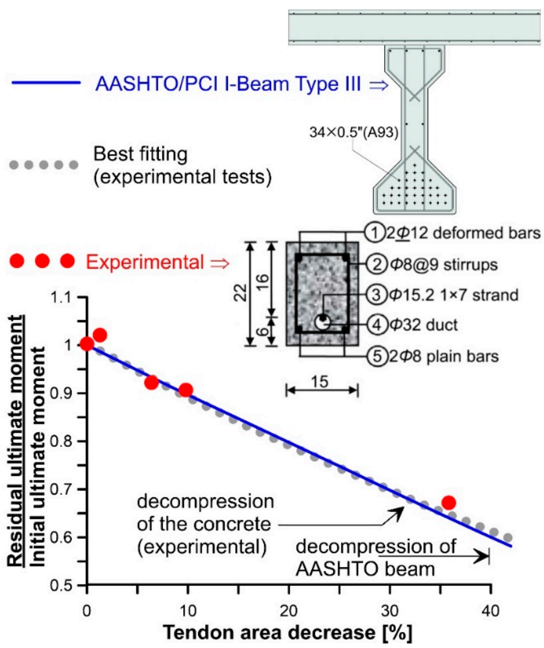

Figure 8. Variation of the ultimate moment at the decrease of the tendon area.

4.3. Failure Probabilities Comparison between the Reinforced and the Prestressed Concrete Section

A further comparison between the two sections is provided by Figure 9, that reports the probability of failure P_f as a function of the bridge age. This comparison of the failure probabilities is functional to the discussion that will be reported in the next section. For the sake of simplicity and without loss of generality for the discussion, the computation of the failure probability is restricted to a single flexural failure mode of the beam with the highest value of the bending moment, under uniformly distributed loads.

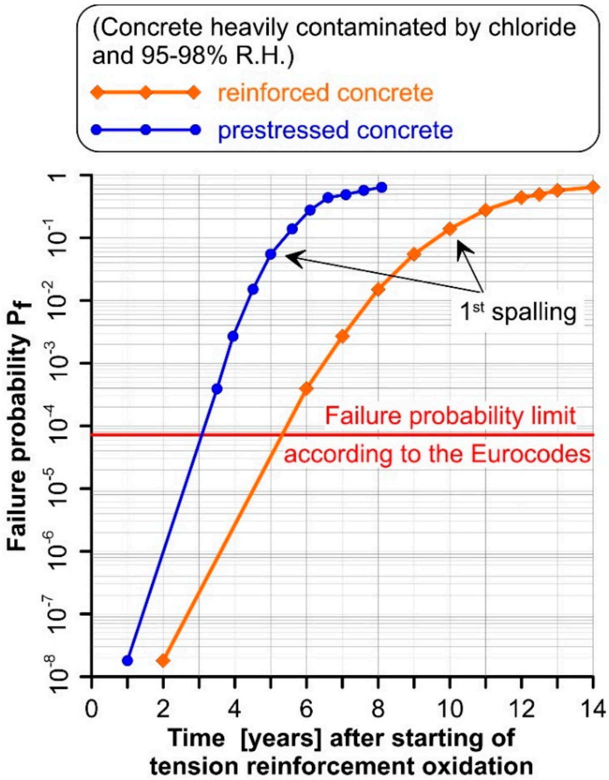

Figure 9. Failure probability versus progress of corrosion.

The cross-sectional capacity is computed as $C = C_{mod}\theta$, where C_{mod} is the value of capacity obtained with the numerical model and θ is the model uncertainty, which is a random variable. The properties of the model uncertainty can be found in [53] for bending resistance models for nondeteriorated and corrosion-damaged RC beams. The model uncertainty θ for nondeteriorated beams is modeled as a Lognormal random variable with 1.07 mean and 0.08 Coefficient of Variation (CoV). The model uncertainty θ for deteriorated beams is modeled as a lognormal random variable with mean 0.99 and CoV 0.10. The cross-sectional capacity is computed as in Section 4 for increasing corrosion levels. Only variable loads due to traffic are considered. The maximum traffic load is modeled according to [53] using a Gumbel distribution with mean value $0.7X_k$, where X_k is the characteristic value of the traffic load according to the Italian building code (load pattern 1) and CoV 0.075.

The results in Figure 9 relate to very aggressive exposure conditions assuming that the time of initiation of the corrosion is $t = 0$. As expected, the P_f is much higher for the prestressed concrete bridge when compared to the reinforced concrete bridge of the same age. Furthermore, it is noted that the P_f set by Eurocodes for new bridges [54] and similar to that adopted by American and Canadian standards [55], is exceeded before concrete spalling.

Figure 10 shows the P_f as a function of the percentage variation of the first natural frequency for the prestressed and the reinforced concrete beam. In both cases the P_f increases considerably for the first level of damage, exceeding the value prescribed by the Eurocodes. The main difference between the two types of beams is that while in the reinforced beam the increase of the P_f corresponds to a variation of about 12% of the first modal frequency, for the prestressed beam the sharp increase in the P_f occurs for an almost negligible variation of the first modal frequency. The latter presents an appreciable change of about 12% only after concrete spalling; that is, when the probability P_f is close to 1.

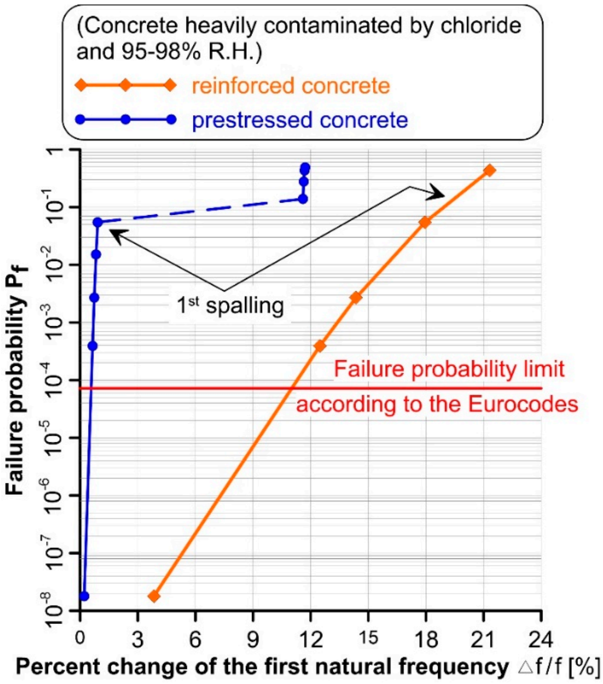

Figure 10. Failure probability versus changes in frequency.

5. Discussion

The comparison between the two types of beams presented in the previous sections shows that modal frequency exhibits a noticeable sensitivity to losses of the tension steel area for reinforced concrete sections and negligible sensitivity for prestressed elements. This result confirms the results of previous experimental tests carried out on prestressed elements, as described in Section 1. The main reason for the different performance is related to the different contributions of the compressed concrete section to the beam bending stiffness. Further to this, and more importantly, the comparison reported in Figures 9 and 10 highlights the main pitfall connected with the use of vibration-based tests to detect damage in prestressed beams. To discuss it, the connection between the information provided by the tests and the decisions involved in structural integrity management must be highlighted.

During the lifecycle of a structure, decisions must be made regarding corrective maintenance actions to control the development of deterioration due to aging or corrosion, for example. The implementation of an efficient maintenance process requires the choice of optimal actions, which are able to minimize the overall service costs over the lifecycle. Bridge management decisions relate both to the type of action and the best time to implement it. A typical decision alternative is to repair as soon as the structure deviates from the design configuration and immediately recover the required level of functionality, or to postpone the remedial action to a later time, thereby accepting a decrease of functionality for a certain time interval, with the benefit of a lower expenditure. In both cases, the collection of information through tests, inspections, or monitoring is aimed to reduce the uncertainty regarding the condition of the structure and thus to support decision making. Keeping this in mind, let us consider the differing behavior of deteriorated reinforced and prestressed concrete. In ordinary reinforced concrete elements, cracking is an inherent aspect of the material behavior. The transfer of tension stresses from concrete to steel entails the cracking of the concrete, which already occurs under service loads. On the other hand, prestressed components are designed to avoid or limit the occurrence of tension stresses on concrete.

As shown by the previous analysis, cracking in such structural elements occurs when the loss of prestress is so high that, under service loads, the beam reliability is consistently lower than the design value. There is thus an essential difference between ordinary and prestressed concrete in terms of the safety level corresponding to the structural state in which damage becomes identifiable using vibration-based tests. This state corresponds to service conditions for an ordinary reinforced concrete section and ultimate conditions for a prestressed beam. For a reinforced concrete section, the results of a vibration-based test can give insight into the actual structural conditions and put bridge operators on alert regarding ongoing degradation processes. As for the prestressed beam, the information on the damage becomes available when the structure is already close to the ultimate condition.

In the Introduction of this paper, it is shown that a large number of studies focused on assessing the sensitivity to damage of vibration-based tests for prestressed beams, demonstrating that they can provide information on damage. The novel contribution of this paper to this topic is the demonstration that, in practice, the information provided by vibration-based tests concerning the onset of damages for prestressed concrete elements becomes available when the structure is already close to collapse. This, added to the scarce sensitivity of modal frequencies to this type of damage, leads to severely doubt the usefulness of these types of tests as decision support tools.

6. Conclusions

Information from monitoring is meant to support decisions regarding possible remedial actions to maintain the required structural performance. Damage detection procedures must thus provide information at the earliest stage of damage development, ideally at the onset of damage, for the interventions to be effectively implemented. In this paper, the feasibility of vibration-based damage detection for prestressed beams is assessed. The performance of modal frequencies as a feature for damage detection in a prestressed beam is assessed and compared with the case of a reinforced concrete beam with similar capacity, using both a simplified analytical approach and a numerical example with refined modeling of corrosion.

Results confirm and explain the scarce sensitivity of modal parameters to damage in prestressed elements reported in the experimental tests discussed in the Introduction. Further to this, the evolution with damage of the probability of failure of the two structural elements highlights that in prestressed elements variations of the modal parameters measurable through vibration-based tests only occur when the structure is close to its ultimate condition. Reinforced concrete beams exhibit a different behavior since the sensible variation of the modal frequencies occurs for moderate damages. This result offers a new perspective to judge the usefulness of vibration-based tests to detect damage in prestressed beams that is not only related to the sensitivity to damage of these damage features. Specifically, in the case of prestressed beams, information concerning the occurrence of damage becomes available when it is "too late", that is when its use to manage the integrity of the beam cannot provide effective results in terms of management choices.

Author Contributions: Conceptualization, M.A.P. and M.P.L.; investigation, P.F.G. and M.P.; supervision, M.A.P. and M.P.L.; writing—original draft, M.A.P., M.P.L. and P.F.G.; writing—review and editing, M.A.P. and M.P.L. All authors have read and agreed to the published version of the manuscript.

Funding: This research was partially funded by the Italian Civil Protection Department within the WP6 "Structural Health Monitoring and Satellite Data" 2019-21 ReLUIS Project.

Data Availability Statement: The data presented in this study are available on request from the corresponding author.

Conflicts of Interest: The authors declare no conflict of interest.

References

1. Fan, W.; Qiao, P. Vibration-based damage identification methods: A review and comparative study. *Struct. Health Monit.* **2011**, *10*, 83–111. [CrossRef]
2. Deraemaeker, A.; Reynders, E.; De Roeck, G.; Kullaa, J. Vibration-based structural health monitoring using output-only measurements under changing environment. *Mech. Syst. Signal Process.* **2008**, *22*, 34–56. [CrossRef]
3. Quqa, S.; Giordano, P.F.; Limongelli, M.P.; Landi, L.; Diotallevi, P.P. Clump interpolation error for the identification of damage using decentralized sensor networks. *Smart Struct. Syst.* **2021**, *27*, 351–363. [CrossRef]
4. Limongelli, M.P.; Chatzi, E.; Döhler, M.; Lombaert, G.; Reynders, E. Towards extraction of vibration-based damage indicators. In Proceedings of the 8th European Workshop on Structural Health Monitoring, EWSHM 2016, Bilbao, Spain, 5–8 July 2016.
5. Giordano, P.F.; Quqa, S.; Limongelli, M.P. Statistical Approach for Vibration-Based Damage Localization in Civil Infrastructures Using Smart Sensor Networks. *Infrastructures* **2021**, *6*, 22. [CrossRef]
6. Kato, M.; Shimada, S. Vibration of PC bridge during failure process. *J. Struct. Eng.* **1986**, *112*, 1692–1703. [CrossRef]
7. Hop, T. The effect of degree of prestressing and age of concrete beams on frequency and damping of their free vibration. *Mater. Struct.* **1991**, *24*, 210–220. [CrossRef]
8. Saiidi, M.; Douglas, B.; Feng, S. Prestress force effect on vibration frequency of concrete bridges. *J. Struct. Eng.* **1994**, *120*, 2233–2241. [CrossRef]
9. Unger, J.F.; Teughels, A.; De Roeck, G. System identification and damage detection of a prestressed concrete beam. *J. Struct. Eng.* **2006**, *132*, 1691–1698. [CrossRef]
10. Capozucca, R. Detection of damage due to corrosion in prestressed RC beams by static and dynamic tests. *Constr. Build. Mater.* **2008**, *22*, 738–746. [CrossRef]
11. Di Evangelista, A.; De Leonardis, A.D.; Valente, C.; Zuccarino, L. Design and testing of corrosion damaged prestressed concrete joists: The Pescara Benchmark. *J. Phys. Conf. Ser.* **2011**, *305*, 012081. [CrossRef]
12. Miyamoto, A.; Tei, K.; Nakamura, H.; Bull, J.W. Behavior of prestressed beam strengthened with external tendons. *J. Struct. Eng. N. Y.* **2000**, *126*, 1033–1044. [CrossRef]
13. Noble, D.; Nogal, M.; O'Connor, A.; Pakrashi, V. The effect of prestress force magnitude and eccentricity on the natural bending frequencies of uncracked prestressed concrete beams. *J. Sound Vib.* **2016**, *365*, 22–44. [CrossRef]
14. Wang, T.-H.; Huang, R.; Wang, T.-W. The variation of flexural rigidity for post-tensioned prestressed concrete beams. *J. Mar. Sci. Technol.* **2013**, *21*, 300–308. [CrossRef]
15. Limongelli, M.P.; Siegert, D.; Merliot, E.; Waeytens, J.; Bourquin, F.; Vidal, R.; Le Corvec, V.; Gueguen, I.; Cottineau, L.M. Damage detection in a post tensioned concrete beam—Experimental investigation. *Eng. Struct.* **2016**, *128*, 15–25. [CrossRef]
16. Zhao, L.; Kim, C.-W.; Goi, Y.; Takemura, K. Vibration-Based Damage Detection for a Prestressed Concrete Box Girder by Means of Subspace Analysis. *ASCE-ASME J. Risk Uncertain. Eng. Syst. Part A Civ. Eng.* **2021**, *7*, 04021056. [CrossRef]
17. Bonopera, M.; Chang, K.C.; Chen, C.C.; Sung, Y.C.; Tullini, N. Experimental study on the fundamental frequency of prestressed concrete bridge beams with parabolic unbonded tendons. *J. Sound Vib.* **2019**, *455*, 150–160. [CrossRef]
18. De Roeck, G. The state-of-the-art of damage detection by vibration monitoring: The SIMCES experience. *J. Struct. Control* **2003**, *10*, 127–134. [CrossRef]
19. Limongelli, M.P.; Tirone, M.; Surace, C. Non-destructive monitoring of a prestressed bridge with a data-driven method. In Proceedings of the SPIE—The International Society for Optical Engineering, Portland, OR, USA, 26–29 March 2017; Volume 10170.
20. Giordano, P.F.; Limongelli, M.P. Response-based time-invariant methods for damage localization on a concrete bridge. *Struct. Concr.* **2020**, *21*, 1254–1271. [CrossRef]
21. Abdel-Jaber, H.; Glisic, B. Monitoring of prestressing forces in prestressed concrete structures—An overview. *Struct. Control Health Monit.* **2019**, *26*, e2374. [CrossRef]
22. Breccolotti, M. Eigenfrequencies of continuous prestressed concrete bridges subjected to prestress losses. *Structures* **2020**, *25*, 138–146. [CrossRef]
23. Cao, L.; Liu, J.; Frank Chen, Y. Theoretical and Numerical Study on the Natural Frequencies of Bridges With Corrugated Steel Webs. *Structures* **2018**, *15*, 224–231. [CrossRef]
24. Breccolotti, M.; Pozza, F. Prestress evaluation in continuous PSC bridges by dynamic identification. *Struct. Monit. Maint.* **2018**, *5*, 463–488. [CrossRef]
25. Aloisio, A. Aspects of Vibration-Based Methods for the Prestressing Estimate in Concrete Beams with Internal Bonded or Unbonded Tendons. *Infrastructures* **2021**, *6*, 83. [CrossRef]
26. Rainieri, C.; Fabbrocino, G. *Operational Modal Analysis of Civil Engineering Structures*; Springer: New York, NY, USA, 2014; ISBN 978-1-4939-0766-3.
27. Katayama, T. Subspace Methods for System Identification. In *Communications and Control Engineering*; Springer International Publishing: Berlin/Heidelberg, Germany, 2005.
28. Chen, B.; Zhao, S.L.; Li, P.Y. Application of Hilbert-Huang transform in structural health monitoring: A state-of-the-art review. *Math. Probl. Eng.* **2014**, *2014*, 317954. [CrossRef]
29. Brincker, R.; Zhang, L.; Andersen, P. Modal identification of output-only systems using frequency domain decomposition. *Smart Mater. Struct.* **2001**, *10*, 441–445. [CrossRef]

30. Quqa, S.; Landi, L.; Diotallevi, P.P. Instantaneous modal identification under varying structural characteristics: A decentralized algorithm. *Mech. Syst. Signal Process.* **2020**, *142*, 106750. [CrossRef]
31. Kullaa, J. Distinguishing between sensor fault, structural damage, and environmental or operational effects in structural health monitoring. *Mech. Syst. Signal Process.* **2011**, *25*, 2976–2989. [CrossRef]
32. Sohn, H. Effects of environmental and operational variability on structural health monitoring. *Philos. Trans. R. Soc. A Math. Phys. Eng. Sci.* **2007**, *365*, 539–560. [CrossRef] [PubMed]
33. Figueiredo, E.; Park, G.; Figueiras, J.; Farrar, C.; Worden, K. *Structural Health Monitoring Algorithm Comparisons Using Standard Data Sets*; Technical Report LA-14393; Los Alamos National Laboratory: Los Alamos, NM, USA, 2009. [CrossRef]
34. Kim, C.W.; Kawatani, M.; Hao, J. Modal parameter identification of short span bridges under a moving vehicle by means of multivariate AR model. *Struct. Infrastruct. Eng.* **2012**, *8*, 459–472. [CrossRef]
35. Kim, C.Y.; Jung, D.S.; Kim, N.S.; Kwon, S.D.; Feng, M.Q. Effect of vehicle weight on natural frequencies of bridges measured from traffic-induced vibration. *Earthq. Eng. Eng. Vib.* **2003**, *2*, 109–115. [CrossRef]
36. Pisani, M.A. Pre-stressing and Eurocode E.C.2. *Eng. Struct.* **1998**, *20*, 706–711. [CrossRef]
37. Quayyum, S.; Hassan, T. Initial Residual Stresses in Hot-Rolled Wide-Flange Shapes: A Computational Technique and Influence on Structural Performances. *J. Struct. Eng.* **2017**, *143*, 04017013. [CrossRef]
38. Jain, S.K.; Goel, S.C. Discussion of "Prestress Force Effect on Vibration Frequency of Concrete Bridges" by M. Saiidi, B. Douglas, and S. Feng. *J. Struct. Eng.* **1996**, *122*. [CrossRef]
39. Pisani, M.A.; Iorio, F.P. Comparative analysis of two precast bridge beams. *Ind. Ital. Cem.* **2004**, *74*, 604–613.
40. CEN. *Eurocode 1—Actions on Structures—Part 2: Traffic Loads on Bridges—EN 1991-2*; CEN, European Committee for Standardization: Brussels, Belgium, 2005.
41. AASHTO. *Standard Specifications for Highway Bridges*, 17th ed.; American Association of State Highway and Transportation Officials: Washington, DC, USA, 2002; ISBN 156051-171-0.
42. CEN. *Eurocode 2: Design of Concrete Structures—Part 1-1: General Rules and Rules for Buildings—EN 1992-1-1*; CEN, European Committee for Standardization: Brussels, Belgium, 2006.
43. Pisani, M.A. A numerical method to analyse compact cross-sections. *Comput. Struct.* **1996**, *59*, 1063–1072. [CrossRef]
44. Luo, Y.; Zhou, S.; Wang, C.; Fang, Z. Effects of cations in sulfate on the thaumasite form of sulfate attack of cementitious materials. *Constr. Build. Mater.* **2019**, *229*, 116865. [CrossRef]
45. Zhao, G.; Li, J.; Shi, M.; Fan, H.; Cui, J.; Xie, F. Degradation mechanisms of cast-in-situ concrete subjected to internal-external combined sulfate attack. *Constr. Build. Mater.* **2020**, *248*, 118683. [CrossRef]
46. Zhou, S.; Ju, J.W. A chemo-micromechanical damage model of concrete under sulfate attack. *Int. J. Damage Mech.* **2021**, *30*, 1213–1237. [CrossRef]
47. Bertolini, L.; Elsener, B.; Pedeferri, P.; Polder, R. *Corrosion of Steel in Concrete: Prevention, Diagnosis, Repair*; Wiley-VCH, Verlag GmbH & Co., KGaA: Weinheim, Germany, 2004; ISBN 9783527603374.
48. Ouzaa, K.; Oucif, C. Numerical model for prediction of corrosion of steel reinforcements in reinforced concrete structures. *Undergr. Space* **2019**, *4*, 72–77. [CrossRef]
49. Pedeferri, P. *Corrosion Science and Engineering*; Springer: Cham, Switzerland, 2018; ISBN 978-3-319-97624-2.
50. Ožbolt, J.; Oršanić, F.; Balabanić, G.; Kušter, M. Modeling damage in concrete caused by corrosion of reinforcement: Coupled 3D FE model. *Int. J. Fract.* **2012**, *178*, 233–244. [CrossRef]
51. Liu, Y.; Weyers, R.E. Modeling the time-to-corrosion cracking in chloride contaminated reinforced concrete structures. *Am. Concr. Inst. Mater. J.* **1998**, *95*, 675–681. [CrossRef]
52. Moawad, M.; El-Karmoty, H.; El Zanaty, A. Behavior of corroded bonded fully prestressed and conventional concrete beams. *HBRC J.* **2018**, *14*, 137–149. [CrossRef]
53. Caspeele, R.; Steenbergen, R.; Sykora, M. *Partial Factor Methods for Existing Concrete Structures*; fib Bulletin No. 80, Germany; 2016; ISBN 978-2-88394-120-5. Available online: https://www.fib-international.org/publications/fib-bulletins/partial-factor-methods-for-existing-concrete-structures-161-detail.html (accessed on 29 November 2021).
54. Koteš, P.; Vičan, J. Reliability Levels for Existing Bridges Evaluation According to Eurocodes. *Procedia Eng.* **2012**, *40*, 211–216. [CrossRef]
55. Thoft-Christensen, P.; Nowak, A. *Principles of Bridge Reliability: Application to Design and Assessment Codes*; Structural Reliability Theory, No. 162, Volume R9751; Deptartment of Building Technology and Structural Engineering: Aalborg, Denmark, 1997.